REPORT DOCUMENTATION PAGE

AFRL-SR-BL-TR-01-

0168

ita sources,
pect of this
5 Jefferson
03.

1. AGENCY USE ONLY *(Leave blank)*	2. REPORT DATE 01 Mar 01	3. Final Report: FROM 01 Sep 96 TO 30 Nov 99

4. TITLE AND SUBTITLE MODELING NONEQUILIBRIUM RADIATION IN HIGH ALTITUDE PLUMES	5. FUNDING NUMBERS F49620-96-1-0091

6. AUTHOR(S)
Iain D. Boyd

7. PERFORMING ORGANIZATION NAME(S) AND ADDRESS(ES) SCHOOL OF MECHANICAL AND AEROSPACE ENGINEERING Cornell University 246 Upson Hall Ithaca, NY 14853	8. PERFORMING ORGANIZATION REPORT NUMBER

9. SPONSORING/MONITORING AGENCY NAME(S) AND ADDRESS(ES) AFOSR/NA 801 N. Randolph St. Arlington VA 22203	10. SPONSORING/MONITORING AGENCY REPORT NUMBER

11. SUPPLEMENTARY NOTES

12a. DISTRIBUTION AVAILABILITY STATEMENT

Approved for public release; distribution unlimited.

13. ABSTRACT *(Maximum 200 words)*
This final report summarizes the research carried out on the development of numerical approaches for simulating the radiation emitted in high-altitude plumes of spacecraft and missiles. In Appendix I, we describe the development of ultra violet radiation model for the hydroxyl radical that is implemented in a particel-based Monte Carlo approach for simulating the plumes. In Appendix II, we describe a plume radiation calculation for the plume of the ammonia arcjet flown on the USAF EXEX flight experiment. The research performed in this grant has led to significant advances in the capabilities for modeling these flows.

14. SUBJECT TERMS MODELING NONEQUILIBRIUM RADIATION IN HIGH ALTITUDE PLUMES	15. NUMBER OF PAGES
	16. PRICE CODE

17. SECURITY CLASSIFICATION OF REPORT	18. SECURITY CLASSIFICATION OF THIS PAGE	19. SECURITY CLASSIFICATION OF ABSTRACT	20. LIMITATION OF ABSTRACT
UNCLASSIFIED	UNCLASSIFIED	UNCLASSIFIED	UNL

FINAL TECHNICAL REPORT

For research supported by
AFOSR Grant F49620-96-1-0091

for the period 09/01/96 to 11/30/99

MODELING NONEQUILIBRIUM RADIATION IN HIGH ALTITUDE PLUMES

prepared by

Iain D. Boyd [1]

School of Mechanical and Aerospace Engineering
Cornell University,
246 Upson Hall
Ithaca, NY 14853.

August 2000

[1] Principal Investigator

Table of Contents

Abstract

This final report summarizes the research carried out on the development of numerical approaches for simulating the radiation emitted in high-altitude plumes of spacecraft and missiles. In Appendix I, we describe the development of ultra-violet radiation model for the hydroxyl radical that is implememted in a particle-based Monte Carlo approach for simulating the plumes. In Appendix II, we describe a plume radiation calculation for the plume of the ammonia arcjet flown on the USAF ESEX flight experiment. The research performed in this grant has led to significant advances in the capabilities for modeling these flows.

Overview

It was the aim of this research to improve prediction of ultra-violet and visible radiation emitted by high altitude missile plumes and by the interaction of spacecraft control thruster plumes with the ambient atmosphere. To improve prediction of radiative emission it is first necessary to establish accurate modeling of the fluid dynamics and chemistry for these flows. This research employs the direct simulation Monte Carlo method (DSMC) to compute the flows that are in a strong state of thermochemical nonequilibrium. For application to these flows, development of the DSMC technique is required in terms of electronic excitation models and in terms of schemes for including trace species. These issues were addressed in this research program.

In the course of the grant, significant progress was made in two areas. The first concerned the development of DSMC for direct prediction of ultra-violet radiation. Technical details are provided in Appendix A which contains a reprint of a paper published in *the Journal of Spacecraft and Rockets*. Briefly, the main accomplishments were: (1) direct simulation of the chemistry of formation of the hydroxyl excited state OH(A); (2) detailed prediction of ultra-violet radiation from hydroxyl for hypersonic flows; (3) direct verification of the kinetics models against experimental data.

The second area of work was conducted in support of the USAF flight experiment called ESEX (Electric propulsion Space EXperiment). On ESEX, a high power ammonia arcjet was fired in space. Flight measurements on the spacecraft included contamination and thermal radiation. Remote observation of the radiation emitted by the arcjet plume were made from a USAF facility in Maui. Detailed DSMC computations were performed using 10 million particles on 32 processors of an IBM SP-2 parallel supercomputer in order to accurately resolve the spacecraft contamination. Technical details are provided in Appendix B which contains a paper presented by Professor Boyd at the AIAA Joint Propulsion Conference held in Cleveland, July 1998.

Detailed Computation of Ultra-Violet Spectra in Rarefied Hypersonic Flow

Koffi K. Kossi† and Iain D. Boyd*

Cornell University, Ithaca, New York 14853

A new nonequilibrium radiation model is described that predicts the ultra-violet spectrum of hydroxyl (OH) from the electronic transition $A \longrightarrow X$ for flow conditions corresponding to the Bow-Shock Ultra-Violet-2 flight experiment. Unlike previous studies, the new model includes the direct analysis of the electronically and vibrationally excited states, OH(A,v'=0,1,2) of hydroxyl in the flow field simulations. The flow field is analyzed using the direct simulation Monte Carlo method. Results are presented for the altitude range from 80 to 100 km, where the Knudsen number varies from 0.036 to 1.3. The computation uses algorithms that improve the numerical resolution of the excited states which typically occur at mole fractions of 10^{-15}. The collisional transfer of rotational and vibrational energies of the electronic state, OH(A), are also studied in detail. It is demonstrated that the usual assumption made in continuum radiation models that the rotational and vibrational temperatures of the electronically excited state are the same as those of the ground state of the bulk flow fails. An important improvement is achieved in the spectral prediction using the new nonequilibrium radiation model and good agreement is obtained between flight data and emission predictions over a range of altitudes.

Nomenclature

A	=	excited electronic state designation or reaction rate constant, m^3 molecule^{-1} s^{-1}
c	=	speed of light, m s^{-1}
E	=	activation energy or energy level of state, J
F'	=	rotational energy, m^{-1}
g	=	statistical weight
G'	=	vibrational energy, m^{-1}
h	=	altitude, km
h	=	Planck's constant, 6.625x10^{-34}, J s
J'	=	rotational quantum number
k	=	rate coefficient, m^3 molecule^{-1} s^{-1}
k	=	Boltzmann constant, 1.38x10^{-23}, J K^{-1}
M	=	a third body species
n	=	species number density, m^{-3}
N	=	species number of particles or temperature exponent in rate coefficient expression

† Research Associate. Mechanical and Aerospace Engineering.
* Associate Professor. Mechanical and Aerospace Engineering. Member AIAA.

1

Q	=	partition function
t	=	time, s
T_t	=	translational temperature, K
T_r	=	rotational temperature, K
T_v	=	vibrational temperature, K
V	=	cell volume, m^3
W	=	particle weight
X	=	ground electronic state designation or mole fraction
θ	=	vibrational characteristic temperature, K
ν	=	frequency, Hz
ρ	=	mass density, kg m^{-3}
τ	=	life time or vibrational relaxation time, s

Subscripts

e	=	electronic index
i	=	particle index
s	=	species index
r	=	rotation index
t	=	translation index
u	=	electronic upper state index
v	=	vibration index
v'	=	upper vibrational state
x	=	colliding particle
0,1,2	=	excited states index
∞	=	initial condition

Superscripts

diss	=	dissociation
ex	=	exchange
form	=	formation
qu	=	quenching
[ ]	=	concentration annotation

Introduction

Ultraviolet diagnostic experiments have been carried out to measure the intensity and spectral distribution of the radiation emitted from the shock wave of a missile flying at 5.1 km/s (BSUV-2, Ref. 1) and to validate aerodynamics and radiation transfer models related to reentry conditions. Detailed spectral measurements from BSUV-2 are available from about 110 km to 71 km with uncertainty of a factor of about 2.[1]

The Knudsen number range for flow over the 10 cm radius nose of BSUV-2 varies from about 1 to 0.001. Therefore, numerical simulation of these flows is difficult due to the thermochemical nonequilibrium conditions and the emission predictions signatures can be in error by orders of magnitude. In a previous article,[2] we discussed the prediction of ultra-violet emissions radiated by hydroxyl (OH) for hypersonic nonequilibrium flow conditions corresponding to BSUV-2.[1] The study obtained flow field solutions which include the direct analysis of the electronically excited state species of OH using the direct simulation Monte Carlo method (DSMC). Then, the emission was predicted from the flow field solutions using the nonequilibrium radiation code NEQAIR.[3,4] The present investigation continues these studies with development of a reliable method for predicting the signatures, with the goal of breaking new ground by including the production and quenching of the electronically and vibrationally excited states, OH(A,v'=0,1,2) directly in the DSMC flow field simulations. The effect of rarefaction, and the extremely small mole fractions of the radiating species, about 10^{-9}, have required the development of new algorithms that improve the numerical resolution of the trace species.[2] A further goal of the present study is to take advantage of the direct analysis of the electronic state species to study in detail its rotational and vibrational energies. This allows assessment of the usual assumption made in NEQAIR that the rotational and vibrational temperatures of the excited state species are the same as those of the bulk flow or of the ground state species.

In order to perform the spectral computation, one must first know the number density of the electronically, vibrationally, and rotationally excited states. In the case of an equilibrium condition, this number density is determined from the pressure and the enthalpy. However, for nonequilibrium flow conditions, such a procedure is not possible. Under some conditions, the number densities of the excited states may instead be determined using the Boltzmann distribution for the electronically, vibrationally and rotationally excited states. In addition, as described in Ref. 5, the number density of the electronically excited states can also be calculated by solving the Master equations. The main assumption in this approach is that a quasi-steady state (QSS) exists for the number density of the excited species. The assumption requires the electronic excitation rate coefficients to be much faster than the time scales for diffusion and for changes in overall properties. Under such conditions, the nonequilibrium flow properties, which are the species number densities, the rotational, the vibrational and the electronic temperatures, must be known. Then, the vibrationally and rotationally excited states number densities are computed using the Boltzmann distribution within these levels. However, the present study departs from this approach by computing directly the nonequilibrium number density of the electronically and vibrationally excited states species. This approach allows the direct assessment of the validity of the QSS theory, especially in high altitude regimes where the chemical processes become rare. The present method can also be very useful in helping to understand the nonequilibrium processes that the excited species undergo by providing information about their rotational and vibrational relaxation phenomena. In fact, in NEQAIR, the vibrational, rotational and electronic temperatures of the bulk flow or of the ground state species are used to compute the number density of the electronically, rotationally and vibrationally excited states. In reality, in the conditions of highly nonequilibrium flows, the

3

internal temperatures of the ground state species or those of the bulk flow may be very different from the temperatures of the excited states. In such conditions, the approximation used so far in NEQAIR can lead to errors by orders of magnitude. In the case of the OH molecule, it was found that the ground state species undergoes vibrational energy transfer collisions with rates slower than for the A state, OH(A), by about a factor of 100.[6] Therefore, the main goal of the present study is to develop reliable method for signatures predictions at high altitude conditions.

The outline of the present study is as follows: First, the physical models and numerical algorithms developed for the DSMC analysis are discussed. Then, the nonequilibrium radiation code used in this study is briefly described. The model of vibrational energy transfer of the electronically excited state is introduced. In terms of results, general properties of the DSMC flow field solutions are presented. Results obtained with the new nonequilibrium radiation model are compared with the NEQAIR model. Direct comparison of the predicted peak emissions and spectra with the BSUV-2 data are presented. Finally, the flow field properties that include the rotational and vibrational temperatures of OH(A) are presented and the emission predictions are analyzed in terms of the OH(A) rotational temperature dependence.

Numerical models

The numerical models employed in the present work are described in this section. The physical models implemented in the DSMC code are first considered. The new nonequilibrium radiation model is then introduced and finally, the vibrational energy transfer of OH(A) is presented.

Physical models

The DSMC code employed in the present study is based on the vectorized algorithm described in Ref. 7. The code includes finite rates of rotational and vibrational relaxation, and dissociation, exchange, and recombination chemical reactions. A key development in the code is the implementation of a numerical weighting scheme that allows accurate and efficient simulation of trace species.[8] For the altitude range of interest here, the weighting scheme is needed to resolve the excited states, OH(A,v'=0,1,2) and their precursors, OH and H_2O. It will be found from computations that the electronically and vibrationally excited state species, OH(A,v'=0,1,2) exist in the flows at mole fractions of less than 10^{-9} and these conditions are handled efficiently by the new weighting scheme. However, in order for any OH(A,v'=0,1,2) particles to exist in the flows, they must be produced through collisional excitation. For the altitudes of interest here (80 to 100 km), there are few intermolecular collisions and therefore the occurrence of possible collision events is very rare. As described in Ref. 2, whenever a collision involving an OH particle has sufficient energy to allow electronic and vibrational excitation, the reaction probability is set to unity. The numerical weights of the products are then adjusted to ensure conservation of mass. A special procedure is employed for these excitation collisions whereby several OH(A) particles are created instead of just one. Once again, the numerical weight of each particle is adjusted to conserve total mass. Using this procedure, it is possible to

maintain thousands of OH(A,v'=0,1,2) particles in the simulation. The spontaneous de-excitation reactions:

$$OH(A, v' = 0, 1, 2) \rightarrow OH + h\nu \tag{1}$$

and the predissociation reaction:

$$OH(A, v' = 2) \rightarrow O + H \tag{2}$$

are implemented in the DSMC code using the algorithm described in Ref. 2.

The observed OH ultra-violet emission is from the $A \longrightarrow X$ transition only. Therefore, it is relatively simple to include the production and quenching of the electronically and vibrationally excited states directly in the DSMC flow field simulations. An 11-species reacting flow model is employed for the following species: N_2, N, O_2, O, NO, and H_2O, OH, H, and electronically and vibrationally excited states OH(A,v'=0,1,2). The maximum vibrational levels in the computations is fixed to v'=2 because the experimental spectra show no features of vibrational levels greater than 2. In addition to the air reactions,[7] the hydrogenated species undergo the reactions listed in Table 1. Note that the quenching and de-excitation coefficient rates are from Ref. 4 and the reverse reactions coefficient rates are then computed using the principle of balance at equilibrium. The reactions are simulated by the DSMC code using the total collision energy form of the Generalized Collision Energy model.[9] In previous studies,[2,10] it was shown that prediction of ultra-violet emissions was sensitive to the model assumed for interaction of the gas with the vehicle surface. It was found in Ref. 10 that the best agreement of prediction with experimental data occurred for the translational accommodation coefficient of 0.85. This value is consistent with molecular beam experiments. The rotational and vibrational accommodation coefficients were then set respectively to 0.5 and 0.1. The rotational accommodation coefficient is also consistent with observed molecular beam, and the vibrational accommodation coefficient was estimated. In the present work, these values are retained and the surface temperature is taken as 500 K as measured during the BSUV-2 flight. It is also shown in Ref. 2 that the prediction of ultra-violet emission for OH was sensitive to the free stream concentration. Therefore, the concentrations of the hydrogenated species obtained from a model atmosphere,[11] and used in Ref. 2 are retained here and listed in Table 2.

Nonequilibrium Radiation model

The nonequilibrium radiation code described in Ref. 3 and employed for prediction of emission from flow field solutions, was discussed and verified in Ref. 4 for OH comparing the measured spectra with the predicted emissions. The common assumption made in the NEQAIR code is that the quasi-steady-state (QSS) exists for the number densities of the electronically excited species and a single rotational and vibrational temperature model is employed. The validity of the QSS assumption for high altitude flows was assessed in Ref. 2 using the number density of electronic state species from the DSMC computation. In that approach, the number density of the rotationally and vibrationally excited state was computed using the Boltzmann distribution. The number density of the upper state in the spontaneous emission modeling is then written as

$$n_u = n_e \frac{(2J'+1)}{Q_{vr}} exp[-\frac{hc}{k}(\frac{G'(v')}{T_v} + \frac{F'(J')}{T_r})] \tag{3}$$

where n_e represents the number density of the electronic state. The present work, however, departs from this approach by calculating directly from the DSMC code the number densities of the electronically and vibrationally excited states. In this new approach, the number density of the upper state is written as

$$n_u = n_{v'} \frac{(2J'+1)}{Q_r} exp[-\frac{hc}{k}(\frac{F'(J')}{T_r})] \tag{4}$$

In addition to assessment of the QSS assumption, the new model allows direct assessment of the usual assumption made in NEQAIR that the rotational and vibrational temperatures of the excited state are the same as those of the bulk flow or of the ground state species.

Rotational and vibrational energy transfer of OH(A)

Collisional transfer of rotational and vibrational energies of OH(A) are the topic of interest in this section. Simulating directly in the DSMC code the production and quenching of OH(A), provides the opportunity to study in detail the rotational and vibrational energy transfer. From the exchange reaction:

$$OH(A, v' = 1) + M \rightarrow OH(A, v' = 0) + M \tag{5}$$
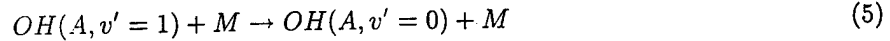
where, $M \equiv N_2, O_2$
we can define the vibrational relaxation time, τ as

$$1/\tau = n_x K_{10}(1 - exp(-\theta_v/T) \simeq n_x K_{10}\theta_v/T \tag{6}$$

where K_{10} is the vibrational excitation rate related to the v' = 1 → 0 vibrational transition cross sections which are reported in Ref. 4 and listed in Table 1. The vibrational relaxation times of OH(A) and OH with N_2 as a colliding partner are shown in Fig.1. It is noted that the vibrational relaxation time of OH(A) is orders of magnitude lower than that of OH which indicates the OH vibrational energy transfer rate to be slower than for the A state, OH(A). The rotational relaxation times of OH and OH(A) are assumed to be the same.

The rotational and vibrational energy transfer are then implemented in the DSMC code in addition to the other molecules using the algorithms described in Refs. 12 and 13. However, for vibrational energy transfer modeling, care must be taken when simulating both vibrational energy exchange and chemical exchange reactions between OH(A,v'=0,1,2). In fact, the exchange reaction processes involving OH(A,v'=0,1,2) also characterize the vibrational energy exchange phenomena. Since the vibrational levels of OH(A) are each treated as if they were separate chemical species and the vibrational relaxation is then treated as a chemical reaction, no additional vibrational relaxation process is applied to OH(A).

Results

6

The presentation of results is divided into three sections: (1) variation of flow field properties over the altitude range of interest; (2) comparisons of predicted emissions using the new nonequilibrium radiation model with the NEQAIR model predictions and BSUV-2 flight data; and (3) presentation of general flow properties including OH(A) rotational and vibrational temperatures and sensitivity of predicted emissions to OH(A) rotational temperature.

As in the previous computational studies of the BSUV-2 flight, only flow over the 10 cm radius spherical nose of the vehicle is simulated. The velocity is in every case 5.1 km/s, and four different altitudes are considered: 80, 88, 94, and 100 km. The hydrogenated species mole fractions, obtained from a model atmosphere presented in Ref. 11. are listed in Table 2. In all cases, the accommodation coefficients for the three energy modes (translation, rotation and vibration) are set respectively to $\alpha_t=0.85$, $\alpha_r=0.5$, and $\alpha_v=0.1$ and the surface temperature is taken as 500 K as measured during the BSUV-2 flight. It is also necessary to note that the values of the accommodation coefficients of the internal energy modes do not influence the radiation prediction.

Flow field Properties

The computed temperatures and number densities are shown in Figs. 2a through 3b for altitudes of 80 and 100 km respectively. The results show the shock layer becoming thicker at higher altitudes and that a large degree of thermal nonequilibrium exists for the altitudes investigated. At 80 km, the extent of the chemistry for some of the species is illustrated in Fig. 2a where OH and OH(A,v'=0,1,2) number densities profiles are included. However. at 100 km altitude, the number densities of species are almost flat indicating the relative importance of diffusion over chemical processes and the peak number density of OH(A,v'=0) is reduced from 10^{12} m^{-3} at 80 km to about 10^7 m^{-3} at 100 km. The peak values of the temperatures are also considerably reduced indicating the effect of rarefaction. The effect of rarefaction is also illustrated in Fig. 3a by the OH(A,v'=2) number density profile. In fact, for any OH(A,v'=2) particle to exist in the flow, it must be produced through OH(A,v'=0) or OH(A,v'=1) collisional excitation. Despite the fact that several OH(A,v'=2) particles are assumed to be created at each collisional event, very few OH(A,v'=2) particles are simulated after several thousand time steps. Note that, despite the efficiency of the numerical model in handling the trace species simulation, the statistical noise related to OH(A) properties are significant. For clarity of presentation, the shock layer domain is reduced in Figs. 3a and 3b. This explains the fact that the temperatures do not reach the free stream value.

In Figs. 2b and 3b, the vibrational temperature of OH(A) is computed from the predicted number density, n_o of the ground state, OH(A,v'=0), and the first excited state, OH(A,v'=1) number density, n_1 using the Boltzmann distribution:

$$T_v = -\frac{\Delta E_v/k}{\ln\left(\frac{n_1}{n_0}\right)}$$

where ΔE_v characterizes the difference between the two energy levels. It is noted that the vibrational temperature computed in this manner is relatively constant.

OH Emission

In Figs. 4a and 4b, the computed spectra at 80 and 100 km are compared with the results obtained using the QSS theory. It is shown that the spectra computed using the QSS theory do not simulate the vibrational transition of OH(A) 1-0 at 0.28 μm and the shoulder of the OH(A) 0-0 vibrational transition at 0.31 μm is too narrow. The absence of the 1-0 feature in the QSS theory is explained by the inaccuracy of the vibrational temperature used in this model. Note that the new radiation model does not use the vibrational temperatures, rather the number densities computed from the flow field simulations. The splitting of the 0-0 peak and the left shoulder of the 0.31 μm peak depend on the rotational temperature, and the disappearance of the 0-0 peak at 100 km in both models is due to the small value of the rotational temperature.

In Fig. 5, the spectrum computed with the new model is compared with the BSUV-2 flight data at 100 km. While the comparison is reasonable, the peak value at 0.28 μm in the prediction is relatively small compared to the data and the left shoulder of the 0.31 μm peak has almost disappeared. One possible explanation for the relatively small value of the predicted peak at 0.28 μm is inaccuracy in the OH(A) collision cross sections. In fact, the ratio of the peak heights at 0.28 μm ($v' = 1 \rightarrow v' = 0$) and 0.31 μm ($v' = 0 \rightarrow v' = 0$) depends on the vibrational temperature. The collision cross sections for vibrational energy exchange reactions, listed in Table 1, were measured for temperatures of about 3,000 K and the use of these data for flow conditions with translational temperatures around 10,000 K may lead to errors. The disappearance of the left shoulder of the 0.31 μm peak is explained by the relatively small value of the computed rotational temperature indicating that the simulation cannot predict correctly all spectral features of the data. As shown in Fig. 3b, the rotational temperature is about 1,500 K, whereas the spectral data indicate the rotational and vibrational temperatures to be on the order of 3,000 K and 7,000 K respectively.

The peak emissions at 0.31 μm as a function of altitude are compared in Fig. 6. The experimental data are from the spectra measured by BSUV-2. The spectral peak height at 80 km is derived from calculation and measurement data using physical arguments.[4] The agreement is quite good at all altitudes lying within a factor of 2 at 88 km and about 10 at 100 km. Recall that there is about a factor of 2 uncertainty in the BSUV-2 data.

OH(A) Flow Properties and Emission Sensitivity to Rotational Temperature.

To assess the validity of the single rotational and vibrational temperatures assumption employed in NEQAIR, profiles of bulk flow and OH(A) temperatures along the stagnation streamline are shown in Figs. 7a and 7b for altitudes of 80 and 100 km. Note that the vibrational temperatures obtained through vibrational relaxation of OH(A) and reproduced in Figs. 7a and 7b, are different from the temperatures in Figs. 2b and 3b, which are obtained assuming a Boltzmann distribution. It is seen in Fig. 7b that the

8

internal temperatures of OH(A) are very high in the free steam. This is explained by the importance of the diffusion process. In fact, due to rarefaction effects at 100 km, OH(A) particles produced through chemical processes diffuse all along the stagnation streamline from their point of formation preventing OH(A) internal temperatures from converging to the free stream value. It is also clearly shown that the internal temperatures of OH(A) are different from those of the bulk gas. However, at 80 km where there is a sufficient number of collision events, the two rotational temperatures are very similar. The two vibrational temperatures are quite different; the OH(A) vibrational temperature is very close to its rotational temperature and the peak value is about 7,500 K. At 100 km, simulations show that OH(A) internal temperatures are very high compared to the bulk gas. The OH(A) rotational and vibrational temperature peaks are about 4,000 K and 5,000 K, whereas the bulk gas flow simulation indicates the flow rotational and vibrational temperatures to be about 1,500 K and 800 K respectively (Fig. 3b). The present results also show that the OH(A) vibrational temperature becomes important compared to the rotational temperature in agreement with the BSUV-2 flight experiments. However, the present results are different by about 1,000 K from the spectral data which indicate the OH(A) rotational and vibrational temperatures to be on the order of 3,000 K and 7,000 K respectively. To explain the discrepancy, further results were computed by varying the internal energy mode accommodation coefficients. However, the results obtained for several tests indicate that the internal temperatures do not vary much with accommodation coefficients. It is concluded that the internal temperatures of OH(A) are related to OH(A) chemical processes and this conclusion will be confirmed in the following discussions. In simulating OH(A) production from OH molecules using the generalized collision energy model, any excess collision energy above the activation energy is equipartitioned into the rotational and vibrational modes. This approach is partially verified through the relatively good agreement obtained with the BSUV-2 spectra.

Sensitivity of the emission predictions to the OH(A) rotational temperature is considered here. The new nonequilibrium radiation model is again considered. In contrast to results shown above, the rotational temperature of the bulk gas in the emission prediction is replaced by the OH(A) rotational temperature. As seen from Fig. 8b at 100 km, the splitting of the 0-0 peak and the right shoulder of 0.31 μm peak vary considerably with the rotational temperature. At 80 km (Fig. 8a), this variation is insignificant indicating that the OH(A) rotational temperature is the same as the bulk rotational temperature. In Fig. 9a, the spectrum computed using the OH(A) rotational temperature is compared with the BSUV-2 data at 100 km. An improvement is obtained with the left shoulder of the 0.31 μm peak which has increased significantly in the calculated spectrum. However, this peak value is relatively high compared to the experimental data, which indicates that the OH(A) rotational temperature is too high in the numerical simulation. To assess this conclusion, the emission is predicted at 100 km altitude assuming a rotational temperature of 3,000 K. Figure 9b indicates a decrease of the right shoulder of 0.31 μm peak which is now in good agreement with the BSUV-2 flight data. This result confirms the OH(A) rotational temperature to be on the order of 3,000 K. Using the OH(A) rotational temperature, it is noted that the peak emission at 0.31 μm is reduced, especially

at 100 km where the OH(A) and the bulk gas rotational temperatures have a large discrepancy.

Assuming the rotational temperature of OH(A) to be 3,000 K at 100 km altitude and comparing the predicted peak with the flight data, an estimate of the OH free stream mole fraction is then obtained. The derived OH mole fraction is about 4.0×10^{-9}. This value is about 20 times higher than the value reported in Table 2. Using the same procedure, the free stream water mole fraction is derived at 80 km through comparison of the predicted peak with the derived 80 km data point. The derived water mole fraction is about 6.1×10^{-6} and very close to the data reported in Table 2. It was found in Ref. 2 that at low altitudes such as 80 and 88 km, the emission predictions were directly proportional to the ambient water mole fraction. However, at high altitudes, such as 94 and 100 km where the effects of rarefaction are very significant, the emission predictions were directly proportional to the OH free stream mole fraction. Considering these results, the ambient water mole fraction and the OH free stream mole fraction are also derived at 88 and 94 km. The water mole fraction is found to be on order of 4.2×10^{-6} at 88 km and the OH mole fraction is about 6.0×10^{-9} at 94 km. The derived mole fractions of the hydrogenated species are reported in Table 3.

Using the mole fractions of the hydrogenated species listed in Table 3, the DSMC method is applied to compute the flow field properties, and the new nonequilibrium radiation model is used to predict OH emission over the altitude range of 80 to 100 km. In Fig. 10, the peak emissions at 0.31 μm as a function of altitude are compared with data taken from the spectra measured on the BSUV-2 flight. Clearly, excellent agreement is obtained suggesting that the hydrogenated species mole fractions experienced in the BSUV-2 flight experiments are within the data listed in Table 3. However, as mentioned previously, the quenching coefficient rates can also explain the discrepancy observed between the predicted spectra and the experimental data. The derived mole fractions must then be considered representative rather than definitive.

Considering once again the flow and OH(A) properties at 100 km altitude, it is shown in Fig. 11 that the OH(A) rotational and vibrational temperatures are in good agreement with the temperatures indicated by the BSUV-2 spectral data. It is noted that the internal temperatures of OH(A) obtained with the new free stream mole fraction are higher than those reported in Fig. 7b. In fact, since the OH mole fraction is increased, the occurrence of collisional excitation is also increased and so are the number of particles in high rotational and vibrational levels. This result also demonstrates that, in high altitude conditions, OH(A) internal energy temperatures are related to the chemical processes rather than collisional energy transfer.

Summary

The direct simulation Monte Carlo method was used to predict the number densities of electronically and vibrationally excited state species of OH in nonequilibrium, hypersonic flight conditions. The conditions corresponded to the Bow-Shock Ultra-Violet-2 flight experiment over the altitude range of 80 to 100 km.

The profiles of OH(A,v'=0,1,2) were then used to predict the ultra-violet spectra from OH(A). The comparisons of both the peak value and the overall spectral shape were found to be in good agreement with the flight data. However, the ratio of the peaks at 0.28 μm showed some disagreements which could be related to the inaccuracy of the quenching and exchange collision cross sections at high temperature. In

10

addition, the left shoulder height at 0.31 μm showed disagreements at high altitude which are due partly to inaccuracy in computing rotational temperatures. Nevertheless, the present study represents a significant improvement compared to NEQAIR.

Comparisons of OH(A) rotational and vibrational temperatures with the bulk gas flow values showed that at the lower altitude conditions, the two rotational temperatures were in good agreement while the vibrational temperatures were very different. Furthermore, it was also shown that at high altitude, the OH(A) internal temperatures were higher than the bulk gas. Using OH(A) rotational temperatures, the emission was computed that reproduced both the spectral shapes and the peak emissions dependence on the rotational temperature. Comparisons of the emission predictions with the BSUV-2 flight experiments allowed the estimation of H_2O and OH ambient mole fractions over the range of altitudes of interest. The H_2O ambient mole fractions were found to be close to values from a model atmosphere, while OH free stream mole fractions were found to be higher by about a factor of 20. Using the derived free stream mole fractions, the flow field was then computed and the emissions predicted. Good agreement was obtained with the flight data for both the peak emission and the overall spectra. With the new free stream mole fractions, agreement was obtained between OH(A) internal temperatures and those indicated by the spectral data.

Acknowledgments

References

[1] Erdman, P. W., Zipf, E. C., Espy, P., Howlett, L. C., Levin, D. A., Collins, R. J., and Candler, G. V., "Measurements of Ultraviolet Radiation from a 5-km/s Bow Shock," *Journal of Thermophysics and Heat Transfer*, Vol. 8, No. 3, 1994, pp. 441-446.

[2] Kossi, K. K., Boyd, I. D., and Levin, D. A., "Direct Simulation of Ultra-Violet Emission From the Hydroxyl Radical," *Journal of Thermophysics and Heat Transfer*, Vol. 12, No. 2, 1998, pp. 223-229.

[3] Park, C., "Calculation of Nonequilibrium Radiation in the Flight Regimes of Aero-Assisted Orbital Transfer Vehicles," *Thermal Design of Aero-Assisted Orbital Transfer Vehicles*, edited by H. F. Nelson, Vol. 96, Progress in Astronautics and Aeronautics, AIAA, New York, 1985,.

[4] Levin, D. A., Laux, C., and Kruger, C., "A General Model for the Spectral Calculation of OH Radiation in the Ultraviolet," submitted to *Journal of Quantitative Spectroscopy and Radiative Transport*, Ap 1997.

[5] Park, C., *Nonequilibrium Hypersonic Aerothermodynamics*, Wiley, New York, 1990, pp. 89-118

[6] Copeland R. A., Wise, M. L. and Crosley, D. R.," Vibrational Energy Transfer and Quenching of $OH(A^2\Sigma^+, v' = 1)$," *Journal of Physical chemistry*, Vol. 92, No. 20, 1988, pp. 5710-5715.

[7] Boyd, I. D. and Gokcen, T., "Computation of Axisymmetric and Ionized Hypersonic Flows Using Particle and Continuum Methods," *AIAA Journal*, Vol. 32, 1994, pp. 1828-1837.

[8] Boyd, I. D., "Conservative Species Weighting Scheme For the Direct Simulation Monte Carlo Method," *Journal of Thermophysics and Heat Transfer*, Vol. 10, 1996, pp. 579-585.

[9]Boyd, I. D., Bose, D., and Candler, G. V., "Monte Carlo Modeling of Nitric Oxide Formation Based on Quasi-Classical Trajectory Calculations," *Physics of Fluids*, Vol. 9, 1997, pp. 1162-1170.

[10]Boyd, I. D., Phillips, W. D., and Levin, D. A., "Sensitivity Studies for Prediction of Ultra-Violet Radiation in Nonequilibrium Hypersonic Bow-Shock Waves," *Journal of Thermophysics and Heat Transfer*, Vol. 12, No. 1, 1998, pp. 38-44.

[11]Brasseur, G. and Solomon, S., *Aeronomy of the Middle Atmosphere*, 2nd Edition, Reidel Publishers, Dordrecht, 1986, pp. 442-443.

[12]Bergemann, F. and Boyd, I. D., "New Discrete Vibrational Energy Model for the Direct Simulation Monte Carlo Method," *Rarefied Gas Dynamics*, Vol. 158 of Progress in Astronautics and Aeronautics, edition AIAA, New York, 1994, pp. 174-183

[13]Boyd, I. D., "Analysis of Rotational Nonequilibrium in Standing Shock Waves of Nitrogen," *AIAA Journal*, Vol. 28, No. 11, Nov 1990, pp. 1997-1998

Table 1 OH kinetics mechanism

Reaction	Rate coefficient, m^3 molecule^{-1} s^{-1} $k=AT^N e^{(-E/kT)}$		
	A	N	E/k, K
$H_2O + N_2 \rightarrow OH + H + N_2$	5.81×10^{-15}	0.00	-53,000.0
$H_2O + O_2 \rightarrow OH + H + O_2$	1.13×10^{-07}	-1.31	-59,400.0
$H_2O + O \rightarrow OH + H + O$	1.13×10^{-07}	-1.31	-59,400.0
$OH + N_2 \rightarrow O + H + N_2$	1.25×10^{-15}	0.06	-51,000.0
$OH + O_2 \rightarrow O + H + O_2$	1.25×10^{-15}	0.06	-51,000.0
$OH + O \rightarrow O + H + O$	1.25×10^{-15}	0.06	-51,000.0
$H + O_2 \longleftrightarrow OH + O$	3.65×10^{-16}	0.00	-8,450.0
$O + H_2O \longleftrightarrow OH + OH$	1.13×10^{-16}	0.00	-9,240.0
$OH + N_2 \rightarrow OH(A,v'=0) + N_2$	9.40×10^{-17}	-0.37	-46,600.0
$OH + O_2 \rightarrow OH(A,v'=0) + O_2$	2.70×10^{-15}	-0.37	-46,600.0
$OH + N_2 \rightarrow OH(A,v'=1) + N_2$	2.30×10^{-19}	0.27	-51,173.0
$OH + O_2 \rightarrow OH(A,v'=1) + O_2$	6.68×10^{-18}	0.27	-51,173.0
$OH(A,v'=0) + N_2 \rightarrow OH + N_2$	1.64×10^{-19}	0.50	687.0
$OH(A,v'=0) + O_2 \rightarrow OH + O_2$	4.76×10^{-18}	0.50	450.0
$OH(A,v'=1) + N_2 \rightarrow OH + N_2$	2.17×10^{-19}	0.50	687.0
$OH(A,v'=1) + O_2 \rightarrow OH + O_2$	6.31×10^{-18}	0.50	450.0
$OH(A,v'=0) + N_2 \rightarrow OH(A,v'=1) + N_2$	5.65×10^{-18}	0.50	-4,573.0
$OH(A,v'=0) + O_2 \rightarrow OH(A,v'=1) + O_2$	9.66×10^{-19}	0.50	-4,573.0
$OH(A,v'=0) + N_2 \rightarrow OH(A,v'=2) + N_2$	7.46×10^{-18}	0.50	-9,146.0
$OH(A,v'=0) + O_2 \rightarrow OH(A,v'=2) + O_2$	2.43×10^{-19}	0.50	-9,146.0
$OH(A,v'=1) + N_2 \rightarrow OH(A,v'=2) + N_2$	8.01×10^{-18}	0.50	-4,573.0
$OH(A,v'=1) + O_2 \rightarrow OH(A,v'=2) + O_2$	9.20×10^{-19}	0.50	-4,573.0
$OH(A,v'=1) + N_2 \rightarrow OH(A,v'=0) + N_2$	5.37×10^{-18}	0.50	0.0
$OH(A,v'=1) + O_2 \rightarrow OH(A,v'=0) + O_2$	9.17×10^{-19}	0.50	0.0
$OH(A,v'=2) + N_2 \rightarrow OH(A,v'=0) + N_2$	6.71×10^{-18}	0.50	0.0
$OH(A,v'=2) + O_2 \rightarrow OH(A,v'=0) + O_2$	2.18×10^{-19}	0.50	0.0
$OH(A,v'=2) + N_2 \rightarrow OH(A,v'=1) + N_2$	7.61×10^{-18}	0.50	0.0
$OH(A,v'=2) + O_2 \rightarrow OH(A,v'=1) + O_2$	8.74×10^{-19}	0.50	0.0
Reaction	Einstein coefficient, s^{-1}		
$OH(A,v'=0) \rightarrow OH + h\nu$	1.44×10^6		
$OH(A,v'=1) \rightarrow OH + h\nu$	1.36×10^6		
$OH(A,v'=2) \rightarrow OH + h\nu$	1.35×10^6		
Predissociation reaction	rate, s^{-1}		
$OH(A,v'=2) \rightarrow O + H$	3.70×10^6		

Table 2 Flow conditions

h (km)	ρ_∞ (kg m^{-3})	T_∞ (K)	X_{H_2O}	X_{OH}	X_H
80	2.00×10^{-5}	181	5.6×10^{-6}	4.3×10^{-9}	2.0×10^{-7}
88	5.11×10^{-6}	195	3.0×10^{-6}	1.2×10^{-9}	7.0×10^{-6}
94	1.30×10^{-6}	177	1.2×10^{-6}	3.0×10^{-10}	9.0×10^{-6}
100	5.68×10^{-7}	185	7.2×10^{-7}	2.0×10^{-10}	1.0×10^{-5}

Table 3 Derived freestream mole fractions.

h (km)	X_{H_2O}	X_{OH}
80	6.1×10^{-6}	....
88	4.2×10^{-6}	....
94	....	6.0×10^{-9}
100	....	4.0×10^{-9}

AIAA-98-3505

Modeling the Plume Contamination And Emissions Of An Ammonia Arcjet

I. D. Boyd, K. C. Kannenberg and K. K. Kossi

Cornell University

Ithaca, NY 14853.

D. A. Levin

George Washington University

Washington, DC 20052.

D. P. Weaver

Air Force Research Laboratory

Edwards AFB, CA 93523.

34th AIAA/ASME/SAE/ASEE
Joint Propulsion Conference & Exhibit
July 13-15, 1998 / Cleveland, OH

Modeling the Plume Contamination and Emissions

of an Ammonia Arcjet

Iain D. Boyd[1], Keith C. Kannenberg[2], and Koffi K. Kossi[3]

Cornell University, Ithaca, NY

Deborah A. Levin[4]

George Washington University, Washington, DC

David P. Weaver[5]

Air Force Research Laboratory, Edwards AFB, CA

Abstract

The direct simulation Monte Carlo method is employed to compute cold flows of ammonia for a large arcjet that is to be tested in space in the upcoming ESEX flight experiment. The nozzle flow computation indicates that the flow is almost in thermal equilibrium at the nozzle exit. A very large and expensive computation of the back flow region of the actual spacecraft geometry is performed to provide predictions of mass fluxes that will be measured in flight by quartz crystal micro-balances. It is indicated that contamination of the spacecraft occurs even in regions lying behind a plume shield. A further computation is performed to simulate the interaction of the arcjet plume with the ambient atmosphere. The high impact energy is offset by the very low atmospheric density at the spacecraft operational altitude of 833 km. Nevertheless, it is indicated that ammonia chemistry occurs and the primary products are NH, NH_2, and OH. These species radiate strongly in the ultra-violet. The estimated emission intensities of the molecules are similar to those measured previously *in situ* by a lower velocity reentry experiment. An estimate is also made of the intensity of emission from ammonia. In all cases, it is concluded for the cold flow that none of the emissions will be detectable by the ground based observation facility that is part of the space experiment.

Introduction

Arcjets represent a mature electric propulsion technology that is replacing chemical propulsion engines for orbit maintenance procedures on many satellites. The U. S. Air Force has developed the Electric Propulsion Space Experiment (ESEX)[1] to study several of the effects of using a very high power ammonia arcjet on a spacecraft. The ESEX experiment is part of the ARGOS flight that will orbit the Earth at an altitude of about 833 km. The flight experiment, due for launch in the winter of 1998, includes diagnostic measurements to analyze exhaust plume contamination and radiative heating effects as well as arcjet performance. Remote

---

[1] Associate Professor. Mechanical and Aerospace Engineering. Senior Member AIAA.
[2] Graduate Research Assistant. Mechanical and Aerospace Engineering.
[3] Post-doctoral Research Associate. Mechanical and Aerospace Engineering.
[4] Research Professor. Chemistry. Member AIAA
[5] Research Scientist. Deceased.

optical measurements are also planned from a ground station at Maui. Several arcjet operational modes will be investigated including the cold flow case where the arc is not ignited.

The goal of this paper is to conduct numerical simulations of the cold flow of the arcjet. The primary motivation for these computations is to provide estimates of the contamination on the spacecraft by ammonia that will be measured by quartz crystal micro-balances. Hence, the focus of these computations will be the back flow region behind the thruster exit plane. A secondary focus of the study is to investigate the interaction of the ambient atmosphere with the ammonia jet exhausting from the thruster. In particular, the goal is to estimate the radiative emission generated under these conditions.

The layout of the paper is as follows. First, the arcjet thruster and diagnostics of ESEX are described. Next, the computational approach is discussed. Due to the relatively low densities involved, the direct simulation Monte Carlo method (DSMC)[2] is employed. Discussion of results is divided into separate sections concerning the back flow contamination studies and the radiative emission calculations.

The ESEX Experiment

A schematic diagram of the ESEX hardware is shown in Fig. 1. As described in Ref. 1, ESEX consists of a 26 kW ammonia arcjet with associated hardware and a diagnostics package. The arcjet has a throat radius of 1.9 mm and an exit radius of 12.6 mm. The nozzle half angle is 19°. The nominal flow rate is 0.25 g/s of ammonia. At full power this provides a specific impulse of 800 s and a total thrust of 2 N.

The ESEX hardware, including the diagnostics package, is part of the ARGOS spacecraft. The diagnostics will measure several aspects of thruster operation including: (1) performance, from thrust measured by an accelerometer, (2) thermal radiation, measured using radiometers, and (3) electromagnetic interference using two spiral cavity antennas. Of most interest to the present study is the measurement of exhaust plume contamination using quartz crystal micro-balances (QCM's). These instruments provide species-resolved mass flux data. The QCM's are located in four different positions. QCM's 2 and 3 are located on the diagnostic platform in the back flow region and their inlet planes are parallel to the thruster exit plane. QCM 1 is located on a solar cell witness plate and points towards the thruster. QCM 4 is located on a deployable boom that extends beyond the perimeter of the spacecraft and again its inlet plane is parallel to the thruster exit plane.

The emissions radiated by the arcjet during ignited operation will be measured from a ground-based facility at Maui. From laboratory experiments, the principal spectral features easily observable from the ignited arcjet are expected to arise from electronically excited NH (in the 1st excited, or A, state) in the near-UV at 330-345 nm, and from the Balmer series of hydrogen in the red, blue, and near-UV.[3]

Numerical Simulations

The mass flow rate and physical dimensions of the ESEX thruster indicate that the nozzle flow is in the near continuum regime with a Knudsen number at the throat of about 10^{-4}. By the nozzle exit plane, the Knudsen number has increased to about 10^{-2}. In most of the plume expansion region the Knudsen number

will be significantly higher and the flow is clearly in the rarefied regime. Therefore, all of the computations performed in this study employ the direct simulation Monte Carlo method (DSMC). The DSMC technique has been applied very successfully to a variety of spacecraft propulsion devices including chemical hydrazine thrusters,[4] nitrogen and hydrogen resistojets,[5-6] hydrogen arcjets,[7-8] ion thrusters,[8] and Hall thrusters.[10]

Nozzle Flow

The nozzle flow is computed separately from the plume expansions to reduce computational expense. A DSMC nozzle code from previous resisto-jet studies[4] is employed again here. The computation begins just downstream of the nozzle throat and the initial starting condition is obtained from isentropic theory. All necessary properties are obtained from the flow rate of 0.25 g/s and by assuming a stagnation temperature of 295 K. The computation is performed on a desk-top personal computer using a grid of 1,000 by 100 cells and a total of 500,000 particles. The exit plane profiles of number density, temperature, and velocity are shown in Figs. 2a-2c. They indicate a relatively large boundary layer and thermal equilibrium conditions at the thruster exit. For comparison, data obtained from isentropic theory are also included. The computed specific impulse is 97 sec and the total thrust is 0.24 N. These can be compared with the ignited arcjet performance of 800 sec and 2.0 N respectively.

Plume Back Flow

Accurate plume back flow computations can only be performed with the DSMC technique due to the rapid decrease in density. In this regime, continuum methods simply breakdown, and free molecular, line-of-sight techniques suffer from shadowing effects in the complex geometries of real spacecraft. Obtaining accurate DSMC results for back flow configurations is not easy however since it is difficult to get any significant number of particles into the back flow region. In the present studies, a very large DSMC computation of the arcjet plume expanding onto the ESEX diagnostic platform is performed using a parallel, numerically efficient implementation of the DSMC technique called MONACO.[11] The MONACO code is ideally suited for this application since it uses unstructured grids and provides the user with great freedom in the variation of time steps and particle weights.[12] These attributes make it possible to resolve in a numerically efficient manner the large gradients in density experienced as the gas flows into the region behind the thruster. The computation begins at the nozzle exit plane using output from the nozzle computation. The grid is adapted to make sure the cell size is proportional to the local mean free path everywhere. It is assumed that the plume expands into a perfect vacuum. The total atmospheric number density at an altitude of 833 km is about 10^{12} m^{-3}. This is ten orders of magnitude less than the nozzle exit density as shown in Fig. 2a.

Plume-Atmosphere Interaction

The ESEX arcjet is configured as to fire directly along the velocity vector into the oncoming ambient flow. At an altitude of 833 km, the main constituents in the atmosphere at night are atomic hydrogen (60%), helium (39%) and atomic oxygen (1%). At orbital speed, the collision energy of an ammonia molecule with either helium or oxygen is sufficient to dissociate the ammonia with the heavier oxygen being significantly

more reactive. There are a number of possible chemical channels and some lead to production of NH and OH which are both strong radiators in the ultra-violet. All other species except ammonia will be present only in trace amounts in the plume flow. Procedures for simulating trace species in the DSMC technique have been developed[13] and applied to model OH ultra-violet emission measured in a reentry flight experiment.[14] Those procedures are again used here along with the chemical reaction mechanism shown in Table 1. The table also lists the sources of the reaction rates.

The flow from the arcjet begins at the thruster exit plane using the data from the nozzle simulation. The ambient atmospheric species of H, He and O are introduced at the downstream boundary of the flow domain at orbital speed.

Results

The only results of interest from the nozzle computation are those at the nozzle exit plane and these were presented earlier. As discussed previously, these results are used to start both the contamination and plume emissions studies that are now discussed in detail.

Contamination

The MONACO computation of the impingement of the ammonia plume onto the ESEX payload is performed on 32 processors of an IBM SP-2 computer and uses 11 million particles with 34,000 cells. The large size of the simulation is required to ensure that all of the tenuous back flow region is populated with particles. The grid employed for the computation is shown in Fig. 3a. The locations and orientations of the four QCM's are indicated.

Contours of number density are shown in Fig. 3b. They reveal that the number density decreases by 7 orders of magnitude as the gas flows from the thruster exit to the diagnostic platform. The contours of translational temperature shown in Fig. 3c indicate the regions of expansion and recompression in the complex spacecraft geometry.

Spacecraft surface impingement properties are shown in Figs. 4a and 4b as a function of distance along the spacecraft starting at the lip of the nozzle in the exit plane. In Fig. 4a, it is shown that the mass flux to the ESEX diagnostics platform decreases by 6 orders of magnitude. The locations of QCM's 2 and 3 are indicated. Table 2 lists the mass fluxes predicted at all four QCM locations. QCM locations 2 and 3 are on the platform surface and the predicted mass fluxes are evaluated directly from particles striking that surface. QCM locations 1 and 4 are not located on any solid surface in the simulation and so are evaluated from the product of density and velocity resolved in the direction normal to the QCM inlet face.

In Ref. 1, estimates of the mass fluxes expected at the QCM locations for the ignited arcjet were provided. These are also listed in Table 2 for comparison. It is expected that the mass flux for the cold flow will be greater in the back flow region than that for the ignited flow. This is because the energy from the arc generates very high velocity flow at the nozzle exit creating a well defined, forward moving beam. This conjecture is supported by the predictions for the mass fluxes at QCM locations 1 and 4. For the cold

4

ammonia flow, the mass flux at QCM 4 is two orders of magnitude higher than that estimated in Ref. 1 for the ignited flow. Surprisingly, the predictions for total mass flux onto the diagnostics platform (QCM's 2 and 3) for the cold and ignited flows are almost identical.

In Fig. 4b, the surface pressure is shown to decrease by seven orders of magnitude from the nozzle lip to the diagnostic platform. Clearly, the use of the arcjet in cold flow mode will not produce any significant momentum transfer to the vehicle.

Plume Emission

A total physical domain of 50 cm axially and 25 cm radially is considered. A total of 10,000 cells with 500,000 particles is employed. The simulation is performed on a personal computer.

Contours of the number density of ammonia is shown in Fig. 5a. There is no appreciable sign that the plume has been perturbed by the ambient atmosphere. In contrast, the ambient atoms are clearly interacting with the much denser plume. This is also made clear in Fig. 5b that shows the translational and rotational temperatures of ammonia along the plume axis. Note that the vibrational mode is included in the simulation but is unexcited throughout the nozzle and plume flow.

When the properties of the trace species are investigated, a very different picture of the flow emerges. The level of chemical activity in this highly energetic and rarefied flow is shown in Fig. 6a which presents some of the species number densities along the plume axis. The He profile is almost identical to that for H, and the NH_2 profile is almost identical to that for OH and so for clarity these data are not included. Clearly, the ambient atoms dissociate a small fraction of ammonia molecules into NH_2, NH and OH. The latter two molecules are strong radiators in the ultra-violet, so it is appropriate to estimate the emission that may be generated under these conditions.

The temperatures of the internal modes of OH are shown along the plume axis in Fig. 6b. The very energetic dissociation collisions produce OH molecules that are highly excited. Through subsequent collisions, the translational and rotational temperatures are reduced. However, the vibrational relaxation time is sufficiently slow that almost no further change occurs to the vibrational energy thus leaving OH with a high vibrational temperature. The properties of OH can be compared with those computed in Ref. 14 for BSUV-2 at 100 km. In comparison with the BSUV-2 data, the OH number density shown in Fig. 6a is lower by an order of magnitude, and the translational temperature shown in Fig. 6b is lower by a factor of about 5. Both of these effects will significantly reduce the OH emission generated by the ammonia plume in comparison to the BSUV-2 data. In BSUV-2, ultra-violet spectra were taken at a velocity of 5.1 km/s from 110 km down to about 60 km. While OH emission was detectable *in situ* on BSUV-2, the lower intensity of radiation predicted here for the cold-flow case would not be visible from the Maui facility.

For completeness, the internal mode temperatures of NH are shown in Fig. 6c. The number density of NH is even lower than that for OH while the translational temperatures are similar. It is therefore concluded that the NH emission would not be detectable from the ground.

The calculations did not resolve the vibrationally hot NH_3 molecules that are formed by collisions in

5

the flow with ambient He or O. Also, it is estimated that there are no vibrationally excited NH_3 particles leaving the nozzle. Nevertheless we can estimate the magnitude of the radiation from the cold gas arc-jet flow. The radiance estimates will be compared with those observed by NASA Infrared Telescope Facility[17] of ammonia emission lines from the stratosphere of Jupiter.

Based on the DSMC calculations the main source of radiation for the cold gas mode is if the ammonia itself radiates. The two IR radiation transitions that are considered are those at 2.9 and 10.5 μ with emission rates of 2.2 and 15 transitions/sec, respectively. The radiance from a column of ammonia molecules may be approximated as,

$$I = hc/\lambda \exp(-E/kT) A N \Delta l$$

where A is expressed in transitions/sec, N is the number density of the ground state of ammonia and from Fig. 5a is approximately 1×10^{15} cm^{-3}, and Δl is the layer thickness and is estimated from Fig. 5a to be 20 cm. Figure 5b shows that the translational temperature of ammonia is very cold and is really less than 25 K. However, assuming as an upper limit to radiation a higher value of 75 K, then the radiance of the gas at 10.5 μ is about 3×10^{-11} W/cm^{2}sr. This is a very small number and most likely is not detectable by a remote measurement.

An example of a remote measurement of a similar infrared transition studied radiation from stratospheric ammonia on Jupiter. The data analyses of Kostiuk *et al.*[17] give a column abundance of ammonia of 2×10^{16}/cm^2 which is about the same as in the ammonia arcjet plume. However, the main difference is that the temperature of the Jovian ammonia is 150 K. Using these values in the expression above, a radiance of about 2×10^{-7} W/cm^{2}sr is obtained. This value is four orders of magnitude larger than that estimated for the cold arcjet plume, thereby making it unlikely that a remote measurement could be made. The blackbody radiance at 150 K for this transition (which qualitatively represents the maximum radiance) in the same units is also of order 10^{-7} W/cm^{2}sr. Hence the estimate of the Jovian radiance is qualitatively correct.

The plume flow calculations provide an estimate of the number density of *vibrationallyhot* NH_3 to be about 10^6 /cm^3 with temperatures in excess of 1,000 K. However, use of this estimate does not change the above conclusion that the plume radiance is too low to observe from a remote measurement.

Conclusions

The direct simulation Monte Carlo method was employed to model the nozzle, forward plume, and back flow plume regions of a cold flow ammonia arcjet. The numerical studies were performed for the flight conditions of the ESEX space experiment.

The flow rate and nozzle geometry indicated near continuum conditions for the nozzle flow and this was confirmed by the DSMC computation. A significant boundary layer was formed in the nozzle, but the flow was in thermal equilibrium at the nozzle exit.

The backflow region was well-resolved using a very large DSMC computation. Over 11 million particles

6

were employed in a simulation that ran in parallel on 32 processors of an IBM SP-2. Significant fluxes of ammonia were predicted along all surfaces of the ESEX payload.

Interaction of the ammonia plume with the ambient atmosphere at an altitude of 833 km was also simulated. The ambient atomic oxygen and helium have sufficient energy to dissociate ammonia with the main products being NH_2, NH, and OH. Estimates of the expected ultra-violet emissions from these molecules, and the infra-red emission from the cold ammonia, led to the conclusion that none of the signals could be detected by an Earth-based, remote measurement. It was estimated that the emission from OH would be significantly smaller in magnitude compared to that detected *in situ* by the Bow Shock Ultra-Violet-2 reentry flight experiment.

Acknowledgments

References

[1] Kriebel, M. M. and Stevens, N. J., "30-kW Class Arcjet Advanced Technology Transition Demonstration (ATTD) Flight Experiment Diagnostic Package," AIAA Paper 92-3561, July 1992.

[2] Bird, G. A., *Molecular Gas Dynamics and the Direct Simulation of Gas Flows*, Oxford University Press, 1994.

[3] Johnson, L., private communication.

[4] Boyd, I. D. and Stark, J. P. W., "Modelling of a Small Hydrazine Thruster Plume in the Transition Flow Regime," *Journal of Propulsion and Power*, Vol. 6, 1990, pp. 121-126.

[5] Boyd, I. D., Penko, P. F., Meissner, D. L., and DeWitt, K. J., "Experimental and Numerical Investigations of Low-Density Nozzle and Plume Flows of Nitrogen," *AIAA Journal*, Vol. 30, 1992, pp. 2453-2461.

[6] Boyd, I D., VanGilder, D. B., and Beiting, E.J., "Numerical and Experimental Investigations of Rarefied Flow in a Small Nozzle," *AIAA Journal*, Vol. 34, 1996, pp. 2320-2326.

[7] Boyd, I. D., "Monte Carlo Simulation of Nonequilibrium Flow in Hydrogen Arcjets," *Physics of Fluids*, Vol. 9, 1997, p. 3086.

[8] Boyd, I. D., "Extensive Validation of a Monte Carlo Model for Hydrogen Arcjet Flow Fields," *Journal of Propulsion and Power*, 1997, p. 775.

[9] VanGilder, D. B., Font, G. I., and Boyd, I. D., "Hybrid Monte Carlo-Particle In Cell Simulation of an Ion Thruster Plume," IEPC Paper 97-182, August 1997.

[10] Boyd, I. D. and Longo, S., "Particle Simulation of the D-55 Hall Thruster Plume," AIAA Paper 98-3798, July 1998.

[11] Dietrich, S. and Boyd, I. D., "Scalar and Parallel Optimized Implementation of the Direct Simulation Monte Carlo Method," *Journal of Computational Physics*, Vol. 126, 1996, pp. 328-342.

[12] Kannenberg, K. C., Dietrich, S., and Boyd, I. D., "Development of an Object-Oriented Parallel DSMC Code for Plume Impingement Studies," AIAA Paper 95-2052, June 1995.

[13] Boyd, I. D., "Conservative Species Weighting Scheme for the Direct Simulation Monte Carlo Method," *Journal of Thermophysics and Heat Transfer*, Vol. 10, 1996, pp. 579-586.

[14] Kossi, K. K., Boyd, I. D., and Levin, D. A., "Direct Simulation of High Altitude Ultra-Violet Emission from the Hydroxyl Radical," *Journal of Thermophysics and Heat Transfer*, Vol. 12, 1998, pp. 223-229.

[15] Baulch, D. L., Drysdale, D. D., Home, D. G., and Lloyd, A. C., *Evaluated Kinetic Data for High Temperature Reactions: Vol. 2 Homogeneous Gas Phase Reactions of the H2 -N2- O2 System*, Butterworth, London, 1972.

[16] Yumura, M., Asaba, T., Matsumoto, Y., and Matsui, H., "Thermal Decomposition of Ammonia in Shock Waves," *International Journal of Chemical Kinetics*, Vol. 12, 1980, pp. 439-450.

[17] Kostiuk, T., Buhl, D., Espenak, F., Romani, P., and Bjoraker, G., "Stratospheric Ammonia on Jupiter after the SL9 Collision," *ICARUS*, Vol. 121, 1996, pp. 431-441.

Table 1. NH_3 kinetics mechanism

Reaction	Rate coefficient, m^3 molecule^{-1} s^{-1} $k=AT^N e^{(-E/kT)}$			
	A	N	E/k, K	Reference
$NH_3 + \{He,O\} \rightarrow NH_2 + H + \{He,O\}$	1.41×10^{-14}	0.00	46,507.3	15
$NH_3 + \{He,O\} \rightarrow NH + H_2 + \{He,O\}$	9.13×10^{-15}	0.00	45,754.0	15
$NH_3 + O \rightarrow NH_2 + OH$	6.6×10^{-17}	0.00	4,455.0	15
$NH_2 + \{He,O\} \rightarrow NH + H + \{He,O\}$	9.13×10^{-16}	0.00	37,556.6	15
$NH + \{He,O\} \rightarrow N + H + \{He,O\}$	5.30×10^{-18}	0.50	34,826.6	15
$H_2 + \{He,O\} \rightarrow H + H + \{He,O\}$	5.50×10^{-15}	0.00	52,941.3	15
$OH + \{He,O\} \rightarrow O + H + \{He,O\}$	1.30×10^{-15}	0.06	50,978.0	15
$NH_3 + H \leftrightarrow NH_2 + H_2$	2.10×10^{-16}	0.00	11,065.0	16
$NH_2 + H \leftrightarrow NH + H_2$	3.00×10^{-17}	0.00	2,626.8	15
$NH + H \leftrightarrow H_2 + N$	1.66×10^{-18}	0.00	995.0	15
$NH_2 + NH_2 \leftrightarrow NH_3 + NH$	6.64×10^{-18}	0.00	2,800.0	15

Table 2. Mass flux in kg/m^2/s at the measurement locations.

Arcjet Mode	QCM 1	QCM 2	QCM 3	QCM 4
Cold (present)	5.6×10^{-7}	3.5×10^{-10}	1.8×10^{-9}	2.5×10^{-8}
Ignited (Ref. 1)	3.0×10^{-8}	1.2×10^{-9}	1.2×10^{-9}	1.6×10^{-10}
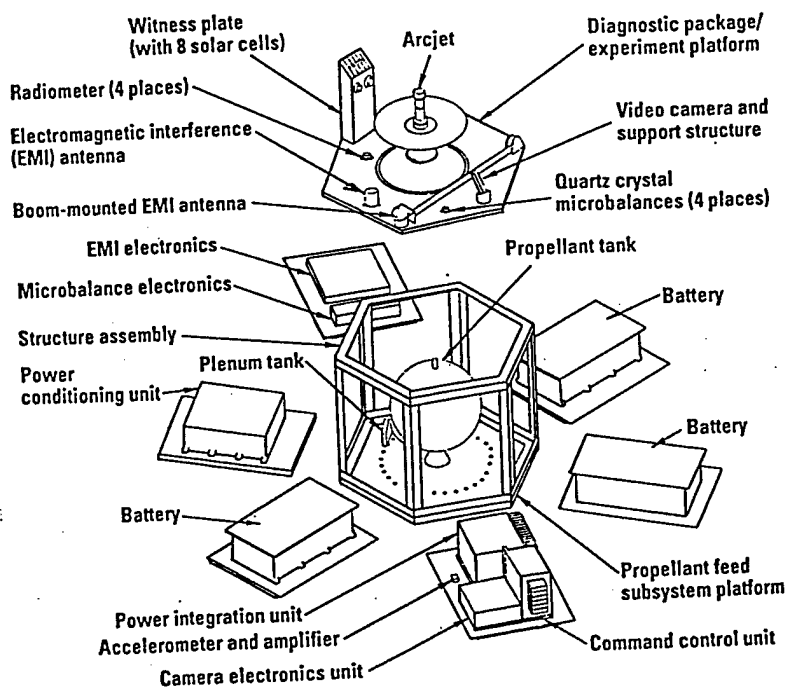
Fig. 1. Schematic diagram of the ESEX experiment.
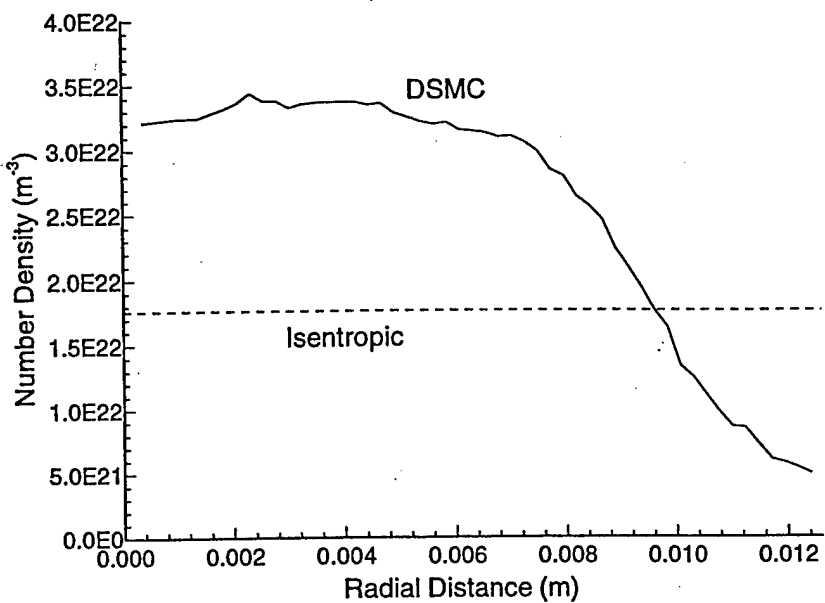
Fig. 2a. Number density of ammonia in the nozzle exit.
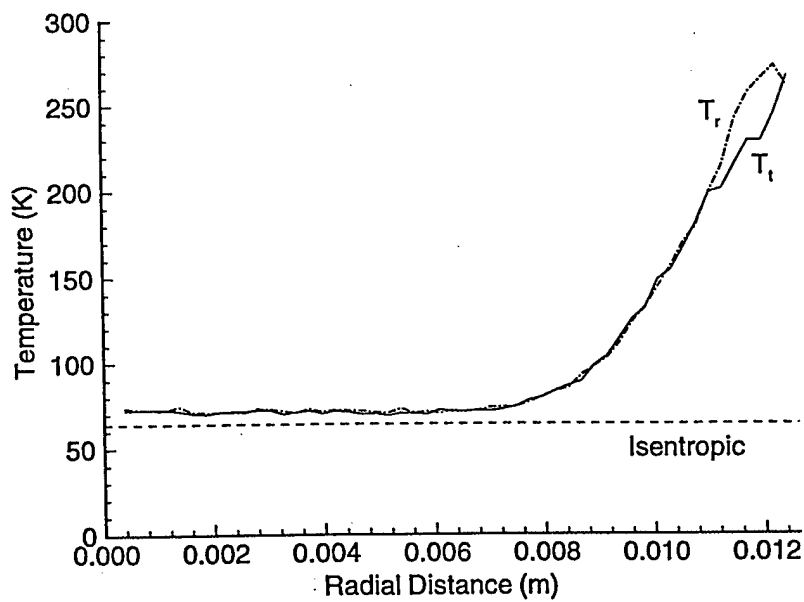
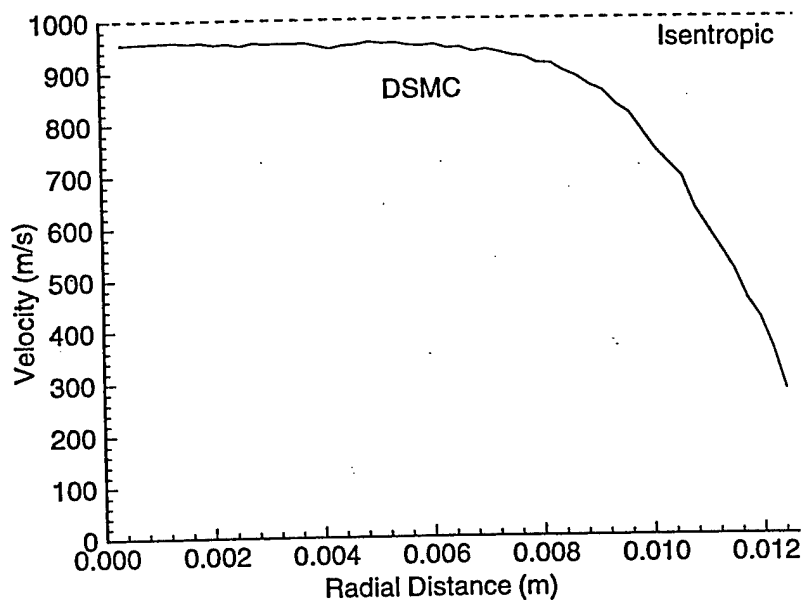Fig. 2b. Temperatures of ammonia in the nozzle exit.
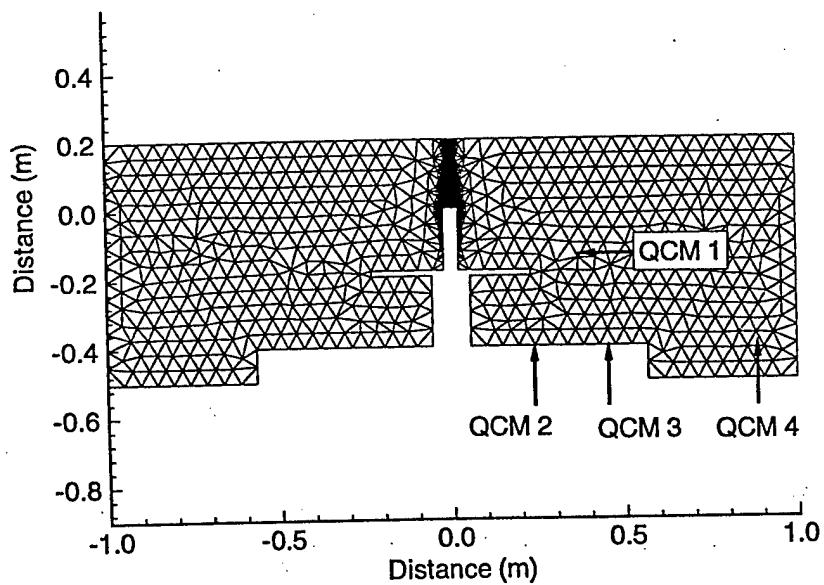
Fig. 2c. Velocity of ammonia in the nozzle exit.

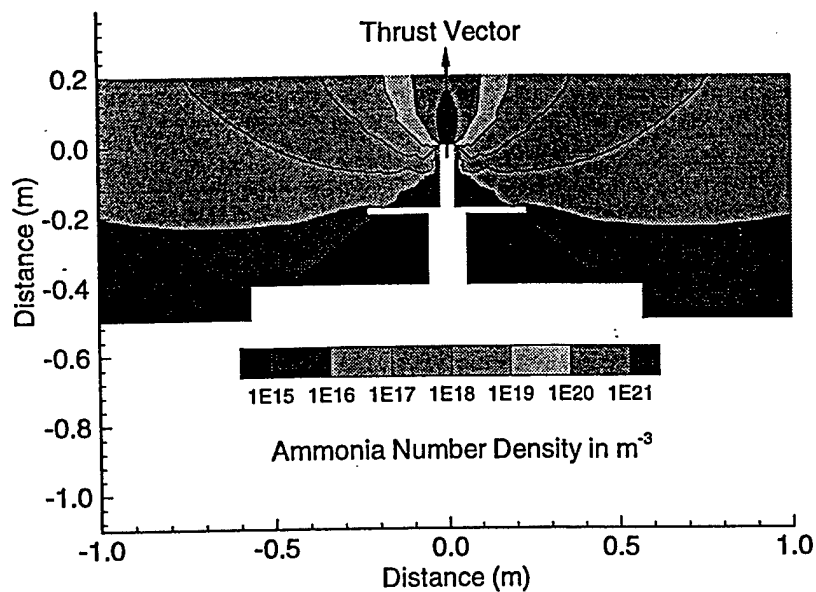Fig. 3a. Grid employed for the contamination simulation.

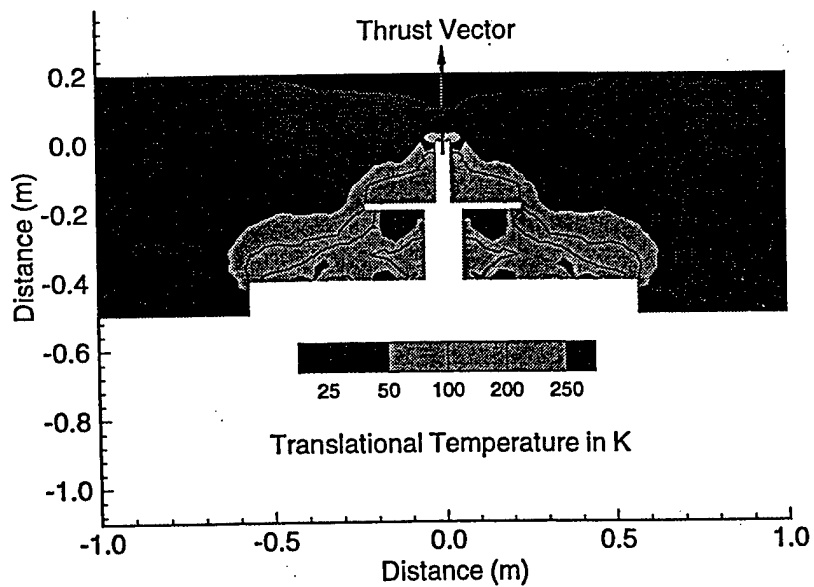Fig. 3b. Number density contours for the contamination simulation.

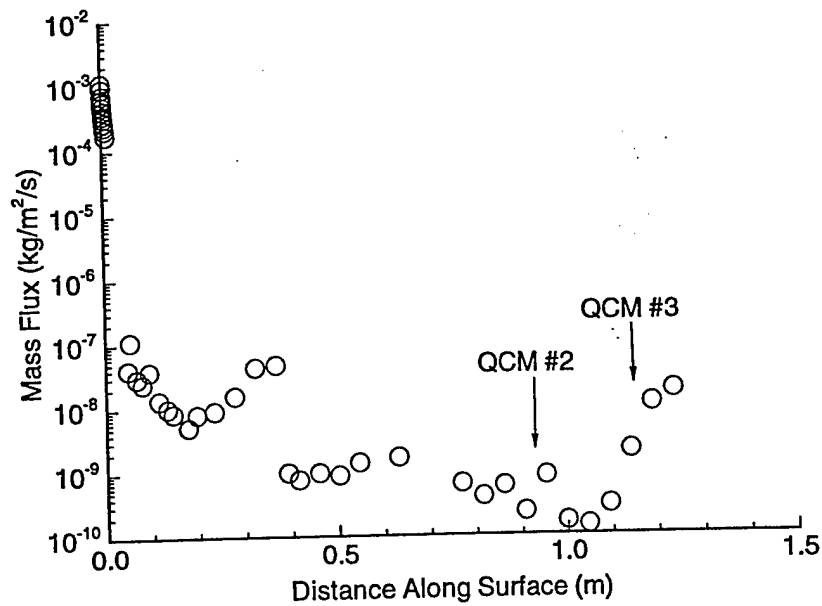Fig. 3c. Translational temperature contours for the contamination simulation.

12

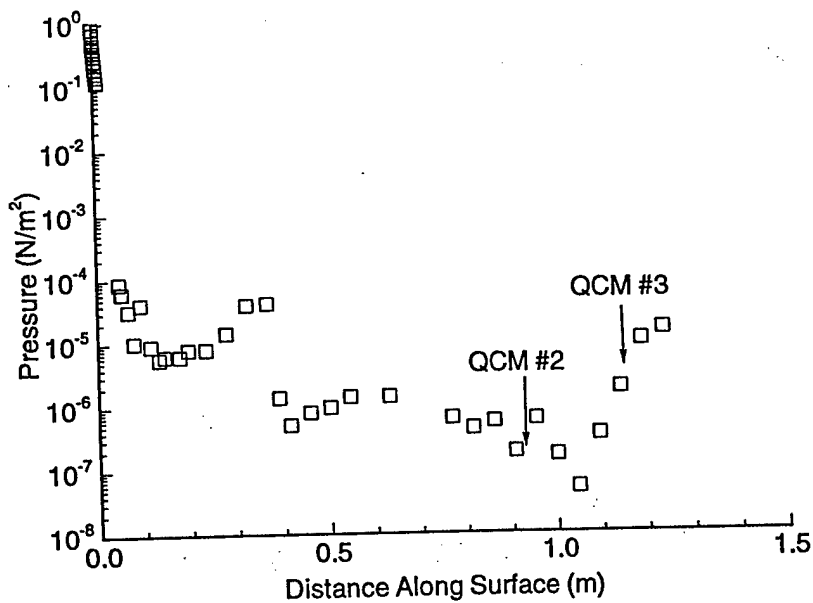Fig. 4a. Mass flux profile along the surface of the ESEX payload starting at the nozzle lip.

Fig. 4b. Pressure profile along the surface of the ESEX payload starting at the nozzle lip.

13
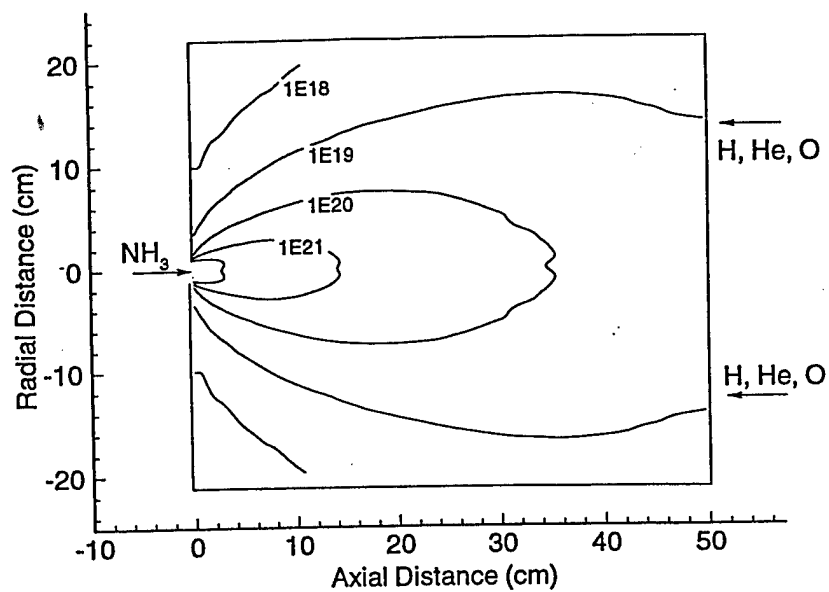
Fig. 5a. Contours of ammonia number density in m^{-3}.
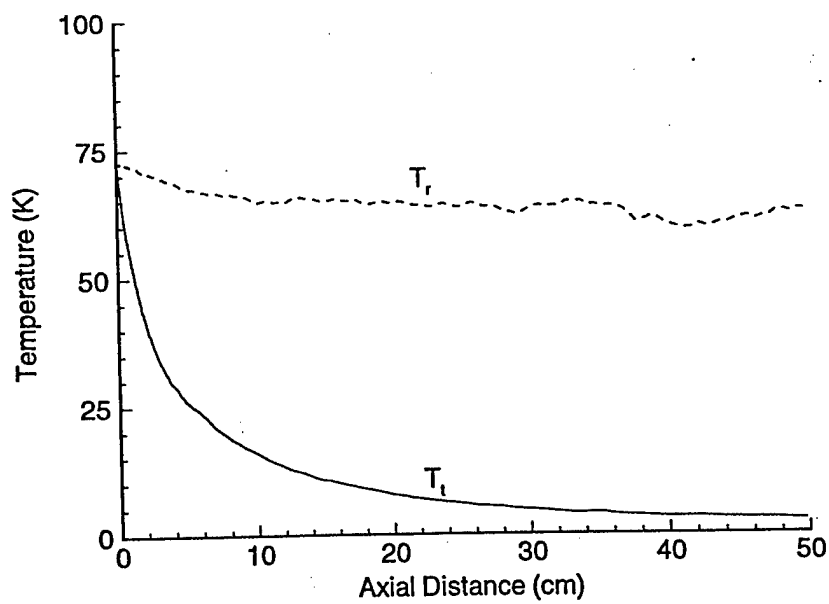
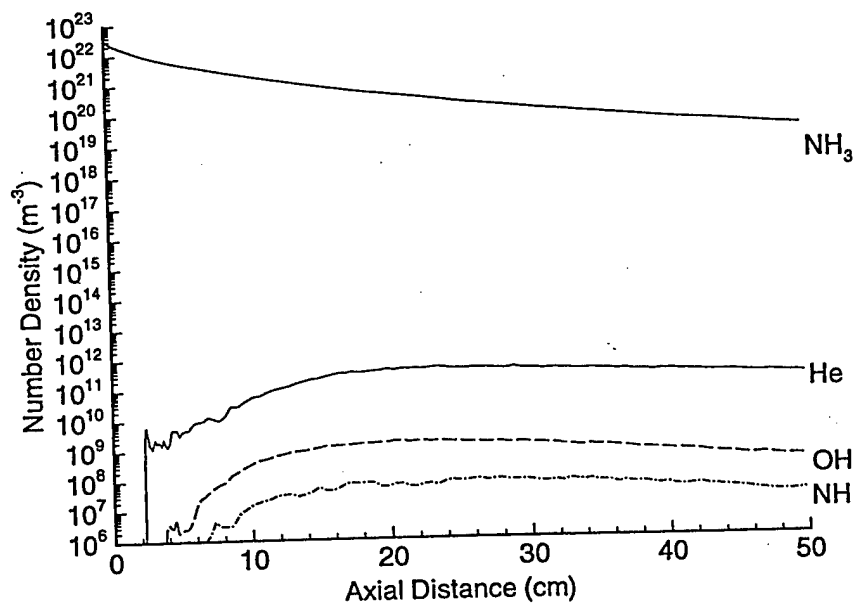Fig. 5b. Ammonia temperatures along the plume centerline.

14

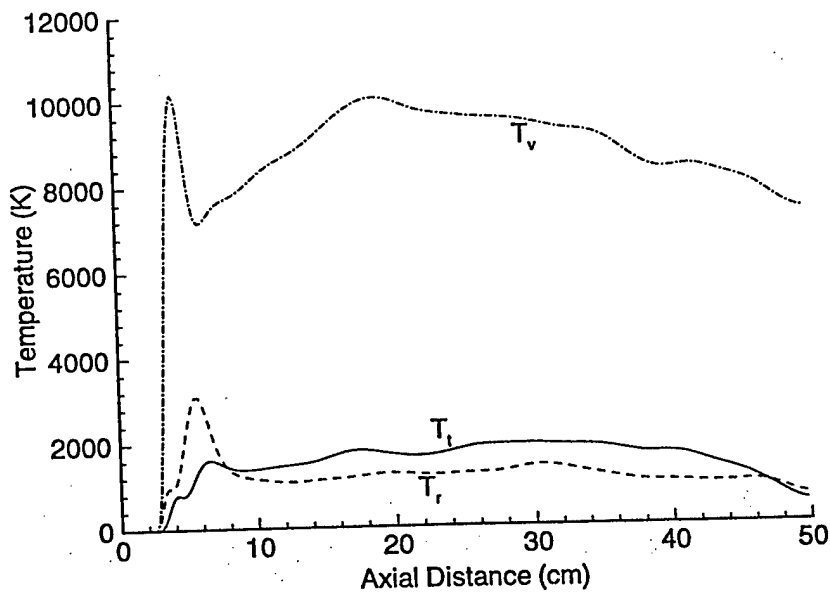Fig. 6a. Number density of selected species along the plume centerline.
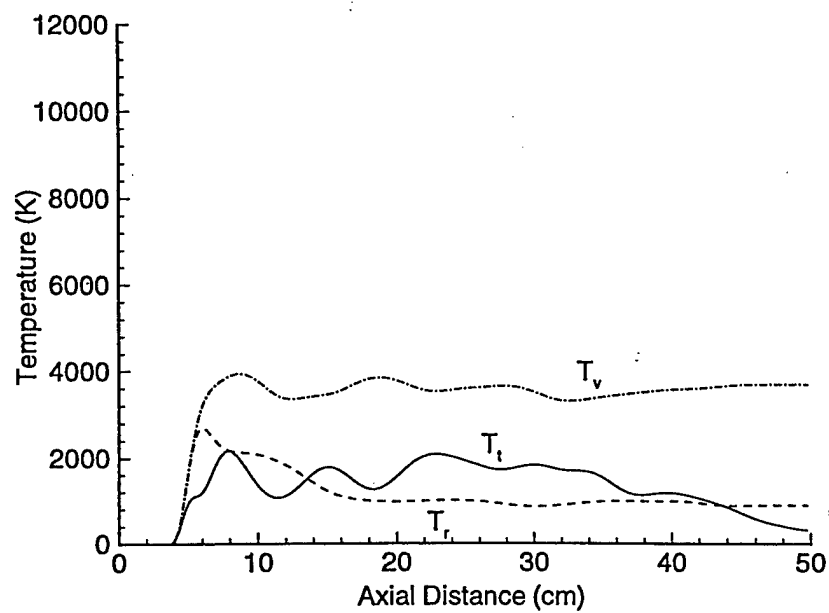

Fig. 6b. Temperatures of OH along the plume centerline.

Fig. 6c. Temperatures of NH along the plume centerline.